Visakhapatnam Chapter

Proceedings of Indian Geotechnical Conference 2020
December 17-19, 2020, Andhra University, Visakhapatnam

Modelling of Diaphragm Wall for Deep Excavation in Sandy Soil

Mandeep Singh[1] and Baleshwar Singh[2]

[1] PG student, Department of Civil Engineering, IIT Guwahati-781039, India
[2] Professor, Department of Civil Engineering, IIT Guwahati-781039, India
[1]singh1234mandeep@gmail.com , [2]baleshwar@iitg.ac.in

Abstract. Modern cities have limited space for new development. Therefore, rising demand for commercial, residential, and industrial needs have driven architects to consider underground structures in their design. Deep excavation is used for basements, subways, and underground car parking in congested cities. The principal types of support systems are diaphragm wall, sheet pile wall, and contiguous pile wall. Among different approaches of design of support systems for deep excavation, the finite element method is becoming popular as it can simulate the construction procedure, movement pattern in the adjacent soil, and effects on adjacent structures. In this study, numerical modelling of a diaphragm wall system with struts for deep excavation in sandy soil has been performed using PLAXIS 2D. The depth of excavation and the groundwater level are 19.6 and 3.5 m, respectively. Lateral deflection of the wall for different excavation phases has been determined along with the influence of interface friction of the wall on lateral deflection, surrounding ground settlement, and surface heave at the base of the excavation. Thereafter, the influence of the depth of embedment of the diaphragm wall and its thickness or stiffness, and mobilised axial force of struts on the maximum lateral deflection of the wall have been studied. Hence, an optimum value can be selected on what demands have to be satisfied such as the permissible lateral deformation of wall and surface settlement or economical considerations.

Keywords: Diaphragm wall; Deep excavations; Finite element analysis; PLAXIS 2D

1 Introduction

Finite element modelling is a great tool in predicting the optimum values required for the design. The accuracy depends on constitutive models and soil parameters. To get soil's effective internal friction angle and soil's stiffness for sand is very difficult because sand samples get disturbed easily. In laboratory tests, effective internal friction angle can be calculated easily as it depends on the shape, compaction, and the surface roughness of sand which are little disturbed but it is difficult to find its stiffness as it depends on intergranular forces between the soil particles and its physical properties which is further depend on the confining pressure or overburden pressure [2–3].

Nikolinakou et al. [5] performed analysis in Berlin sand of an excavation, have done substantial laboratory tests and used the compound elastoplastic model. He observed stress-strain properties depend on the void ratio and effective stress of the recently sand fill. Adequate relation between the calculated deformations and observed deformations observed, but it is difficult to select soil properties and model parameters at the site , practically. Ou et al. [6] used a hyperbolic model, shear wave velocity, and N values for a Taipei silty sand to calculate the stiffness modulus. Hsiung [1] used a Mohr-Coulomb model and equation E=2000xN kN/m^2, in numerical modelling to calculate stiffness modulus of deep excavations in Kaohsiung sand. This correlation is used in this study to get a stiffness of sandy soil in this numerical analysis.
This chapter presents the results obtained from PLAXIS 2D numerical modelling on the Diaphragm wall with struts for deep excavation system in sandy soil. Lateral deflection of the wall for different excavation phases has been determined along with the influence of interface friction of the wall on lateral deflection, surrounding ground settlement, and surface heave at the base of the excavation. Thereafter, the influence of the depth of embedment of the diaphragm wall and its thickness or stiffness, and mobilised axial force of struts on the maximum lateral deflection of the wall have been studied. Hence, an optimum value can be selected on what demands have to be satisfied such as the permissible lateral deformation of wall and surface settlement or economical considerations.

2 Soil Models

Different soil models are available in Plaxis 2D for numerical analysis such as Mohr-Coulomb model, the soft soil model, the hardening soil model, the hardening soil model with small-strain stiffness (HSsmall), soft soil creep model (time-dependent behaviour), modified cam clay model, etc [4]. They can be used depending upon different soil conditions or for comparison purposes. Usually, the Mohr-Coulomb model and hardening model is used widely. In the Mohr Coulomb model, the linear elastic stress-strain curve has occurred, initially and then perfectly plastic curve occurred when the stress states meet the Mohr-Coulomb failure criterion. The slope of the linear elastic curve is called Young's modulus (E). In the HS model, the stress-strain curve is hyperbolic. It contains secant oedometer (E'^{ref}_{50}), effective oedometer stiffness, and unloading–reloading Young's modulus (E'^{ref}_{oed}) at the reference pressure (p_{ref}). To convert these moduli to in situ stress state which are being calculated at the reference pressure Eq. (1) is used.

$$E_{50} = E_{50}^{ref}\left(\frac{\sigma_3^{'}}{p^{ref}}\right)^m \tag{1}$$

where σ'_3, m, $E_{ref}{}^{50}$ are the minor effective principal stress, exponent determining the rate of variation and secant modulus respectively [4,7].

For estimating sand stiffness empirical relationships can be used which required N value and shear wave velocity and used when it is difficult to get the soil stiffness at the site or for the comparison purposes. Various indirect and direct correlations exist between the stiffness of sand and N values. N values directly used to get a stiffness of soil, and in indirect method shear wave velocity is used first to calculate a small strain

dynamic shear modulus, and then it is further used to determine static large strain young's modulus.

3 Site Overview and Characteristics of Soil

An excavation site on which this analysis has been performed is the O6 station of the Kaohsiung transport system and soil characteristics are taken from Hsiung [1]. The length and width of the excavation site at the O6 station are 194 m and 20.7 m, respectively. The maximum excavation depth, diaphragm wall's thickness, and height are 19.6 m, 1 m, and 36 m, respectively. The bottom-up construction method is carried out and W-shaped steel sections are selected as struts members. The depth and width of the flanges are varied from 350 to 414 mm and 350 to 405 mm, respectively. The thicknesses of the flanges and the web thicknesses are varied from 19–28 mm, and 12–18 mm, respectively. For the 3rd, 4th, and 5th level struts, double-W-shaped steel sections are used to provide additional support. The horizontal spacing of the struts is 4.5 m. The soil comprises of up to 60 m of silty fine sand with some small bands of silty clay. The unit weight of the soil and the SPT-N value varies from 18.6 to 20.0 kN/m^3 and 5 to 42, respectively. The groundwater level is 3.5 m below the ground level.

Table 1. Description of ground profile and related soil parameters (Hsiung [19])

Depth (m, below ground level)	Description of soil	Approximate total unit weight (kN/m^3)	Water content (%)
0.0–7.5	Yellow and grey silty sand	19.7	4.9-22.3
7.5–10.0	Grey silty clay with sandy silt	18.6	29.6-41.4
10.0–22.5	Grey silty sand occasionally with sandy silt	19.6	22.9-32.5
22.5–25.0	Grey silty clay with silt	19.3	20.3
25.0–29.5	Grey silty sand with sandy silt	19.7	26.6-30.6
29.5–32.0	Grey silty clay	19.5	28.2
32.0–60.0	Grey silty sand with clay	19.9	22.4-32.2

4 Numerical Modelling

In this analysis, Plane strain two-dimensional triangular mesh elements having fifteen displacement nodes are used in PLAXIS 2D. The lateral boundaries of the model are set as eight times the excavation width away from the diaphragm wall faces. These boundaries are set after performing convergence of boundary conditions as shown in fig.1. The total thickness of the soil layers is 60-m which is defined as the vertical boundary of the model. Bottom boundary movements are restrained. Mohr-Coulomb model is used for the analysis. Total stress undrained analysis is used for the Clay layer. Poisson's ratio value is set to 0.5 so that no volumetric change is there for the clay layer. The Eu (stiffness of soil) is determined using the empirical relation $E_u = 500s_u$ [8] for the clay layers. Effective stress drained analysis is performed for silty sand layers. The soil properties are shown in Tables 1 and 2 for different soil layers. From, $\Psi = \Phi' - 30$ [9] equation the dilation angle is calculated. Poisson's ratio value for the sand layers is set to 0.3 [10]. The linear elastic model is selected for the steel struts and stiffness is determined by EA / L [10] ($E = 2.1 \times 10^8$ kN/m^2), A is the cross-sectional area and L is taken as half of the width of excavation. A fixed anchor element is used, for the struts. To deal with imperfect joint, misalignment, or improper strut installation the strut stiffness should be reduced to 50–70% of the nominal value as suggested by Ou [10]. To model the reinforced concrete diaphragm wall, plate elements are selected. The correlation $E = 4.7 \times 10^6 (f_c')^{0.5}$ [10] is used to determine the stiffness of the wall, where f_c' is the 28-day uniaxial compressive strength of concrete cylinders in MPa. A Poisson's ratio of 0.15 is selected for the wall [4]. To deal with the occurrence of cracks (Due to bending) the stiffness of the diaphragm wall is reduced by 20% [10]. For each excavation level, the groundwater level is maintained 1 m below the excavation bottom in the analysis. The coefficient of permeability of the clay layer and sand layers are set as 0.0001 m/day and 2.333 m/day, respectively [11].

5 Analysis Results

5.1 A convergence of Boundary Conditions

In fig. 2 two sections are observed, first on the ground surface which is 20 m away from the right diaphragm wall because the settlement of ground continuously decreasing as we move away from this point it as shown in fig.5 and another is on diaphragm wall from 10m to 15m depth below G.L during final excavation stage. Now values are taken when a boundary is changed and values are expressed in percentage of excavation depth (De). It is observed that variation starts to parallel when a boundary is increased from 8B (B is the width of excavation) to further. Hence the effect of the boundary is negligible when the size of the soil model is more than 8B (Total width of soil model at 8B is 17B, 8B from each side of sheet pile and B is the width of excavation).

Table 2. Related soil parameters (Hsiung [19])

Depth (m, below ground level)	SPT-N value	C' (kPa)	Ø(˚)	Undrained shear strength (S_u, kPa)
0.0–7.5	5-14	0	32	-
7.5–10.0	4	0	30	28
10.0–22.5	6-22	0	32	-
22.5–25.0	12-16	0	33	98
25.0–29.5	19-29	0	33	-
29.5–32.0	13-19	0	32	112
32.0–60.0	28-42	0	33	-

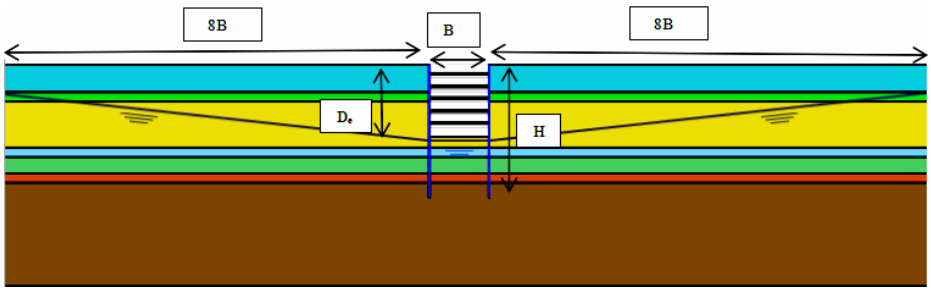

Fig. 1. A numerical model of the diaphragm wall

B (width of excavation)=20.7m

H(Height of diaphragm wall)=36m

D_e(Depth of excavation)=19.6m

5.2 Deformation of Diaphragm wall for different Excavation Phases

Fig.3 shows the deformation of the diaphragm wall for different excavation phases. The maximum horizontal deformation observed in the diaphragm wall is 50 mm under completion of the complete excavation of 19.6m. The deformation of the wall increases as the excavation progresses. Variation of deformation up to excavation depth is linear, it is because of the influence of struts. Axial compressive forces are mobilised in struts with the further excavation that stops further deformation of the wall at the level of struts. It is shown in fig.4. To make sure about results, lateral deformation is validated with Hsiung [1]. After, getting good similarity further analysis has been performed.

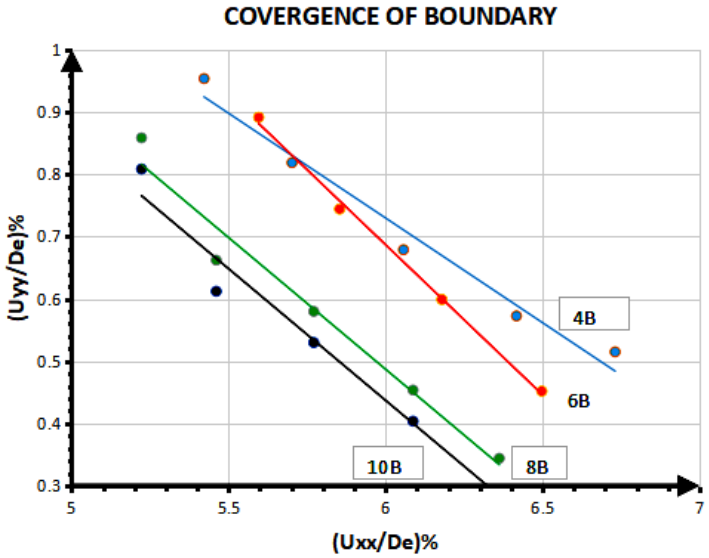

Fig. 2. A Convergence of Boundary Conditions

5.3 Mobilisation of axial compressive forces on Struts with excavation

Fig.4 shows the mobilization of axial compressive force on struts with the progression of lateral deformation of the diaphragm wall. As shown in fig.3, the linear variation of horizontal deformation is due to mobilisation of axial compressive forces in struts. Axial compressive force experienced by struts reduces as other struts take out some of the force of corresponding struts.

5.4 Deformation of the ground surface after final excavation

Fig.5 shows the deformation of the ground surface after the final excavation. The maximum value is observed at 16 m away from the right diaphragm wall which is

26.53 mm. After this distance influence of excavation starts to decrease and approaches nearly zero value at 160 m distance from the wall.

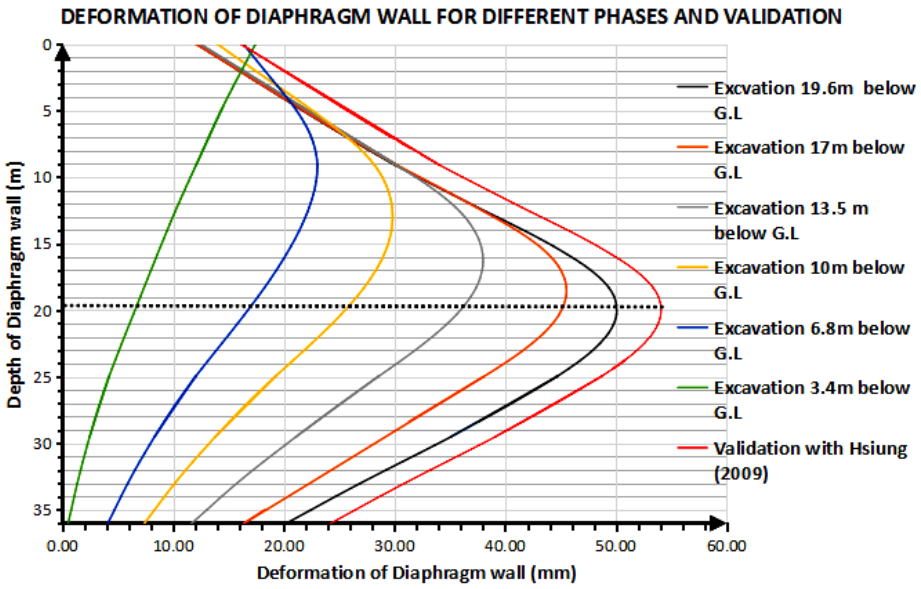

Fig. 3. Deformation of Diaphragm wall for different excavation stages and validation

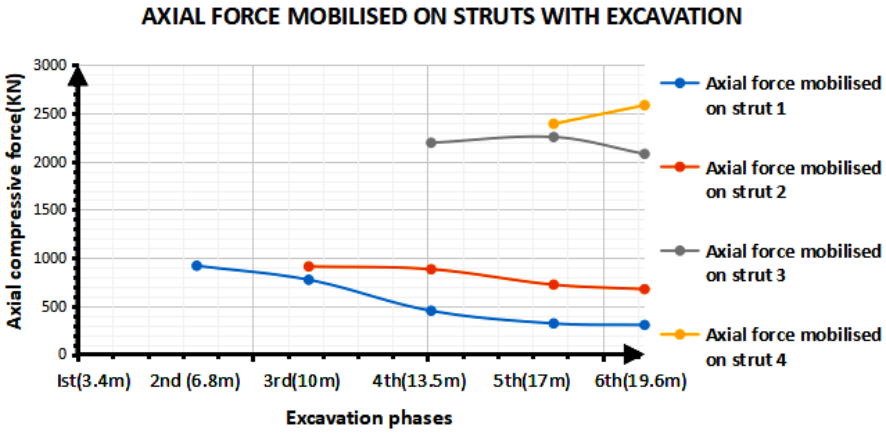

Fig. 4. Mobilisation of axial compressive force on struts with excavation phases

5.5 Deformation of Diaphragm wall for different height of the wall

Fig.6 shows the deformation of the diaphragm wall for different height of the wall (different penetration depth). It is observed that when the height of wall changed to

32m from 36m or when penetration depth reduced to 12.4m from 16.4m (16.4m penetration depth was taken by Hsuing [1]) there is no effect on deformation behaviour so the additional depth of wall can be avoided and when the height of the wall (penetration depth) is further reduced to 28m and 25m there is a small increase in maximum lateral deformation of wall of 2 mm so with the acceptance of this change if it can be bearable in design so that nearby structure is unaffected then penetration depth can be changed to 5.4m from 16.4m. Further reduction from 25m height should be avoided as it brings a change in the maximum lateral deformation of the wall and there is approximate, no passive resistance by the soil beneath the excavation.

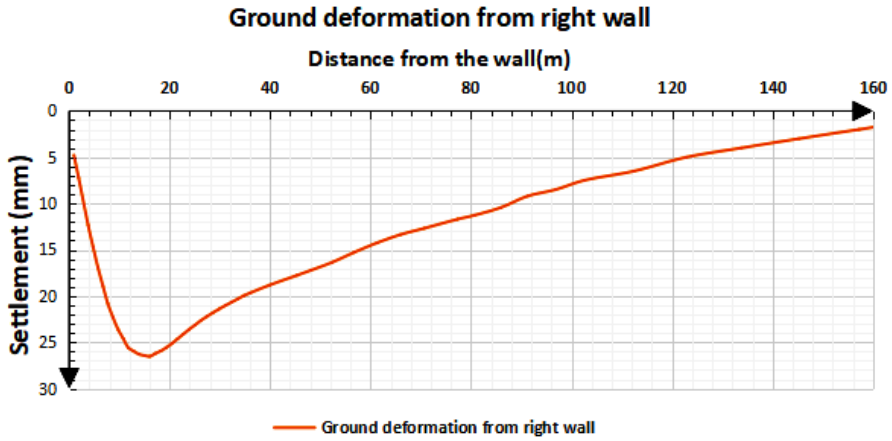

Fig. 5. Deformation of the ground surface after final excavation.

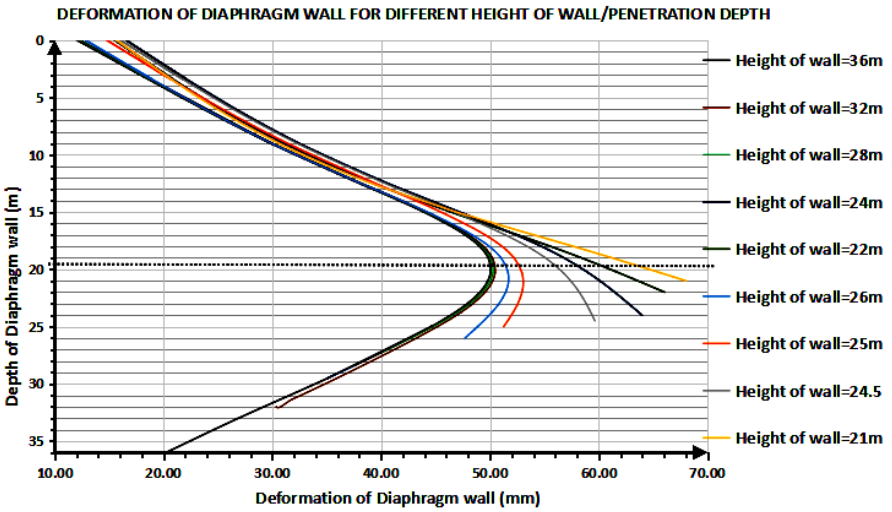

Fig. 6. Deformation of Diaphragm wall for different height of the wall.

5.6 Surface heave at base of excavation for different excavation phases

Fig.7 shows the surface heave at the base of the final excavation level for different phases. For all other phases except the final excavation phase, the observed section is beneath the soil(It is not exposed to the ground). The maximum surface heave observed is 92.865 mm at 10.5 m from the left side diaphragm wall and the observed factor of safety against surface heave is 1.041 so base slab should be constructed as soon as possible to avoid instability conditions.

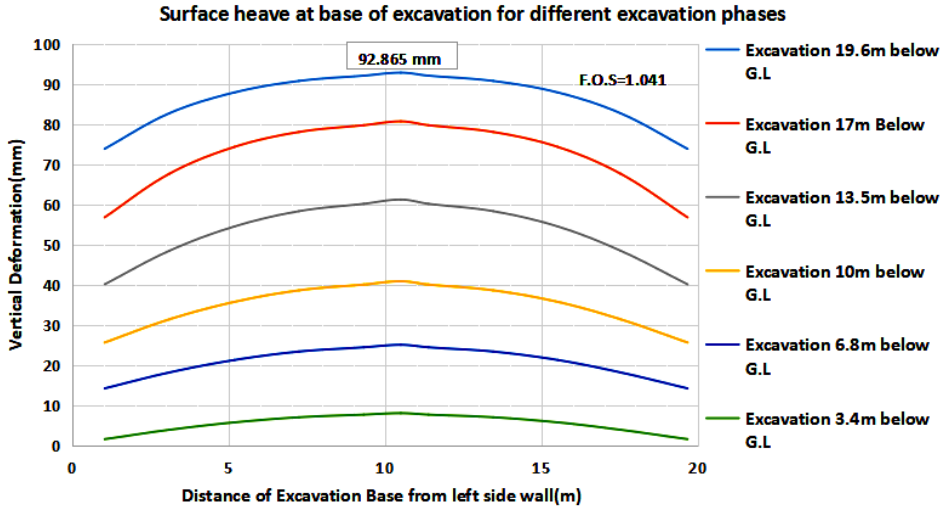

Fig .7. Surface heave at base of final excavation level for different excavation phases.

5.7 Influence of Interface Friction of wall on deformations

Fig.8 shows the influence of interface friction of the wall on deformations. *The* X-axis represents surface settlement (in %) and Y-axis represents wall deformation (in %) after final excavation. They are represented in the percentage of final excavation depth. When the interface friction between the wall and surrounding soil is more as compared to when interface friction is less, fewer deformations (horizontal and vertical) are observed. It means if the wall face towards soil is made rough, fewer deformations of the wall is there.

5.8 Effect of the stiffness of Diaphragm wall on lateral deformation of the wall

Fig.9 shows the effect of the stiffness of the diaphragm wall on the lateral deformation of the wall. The X-axis represents the thickness of the wall in a meter which represents stiffness as the thickness of the wall is directly linked to its stiffness and Y-axis represents lateral wall deformation in mm after final excavation. It is observed

that the curve attains flat as the thickness of the wall is increased. It means the effect of thickness in reducing the lateral deformation of the wall is more when the thickness is less and less when the thickness is more. Lateral deformation reduces only 10mm when thickness increased from 1 to 1.8m (approximately twice its size).

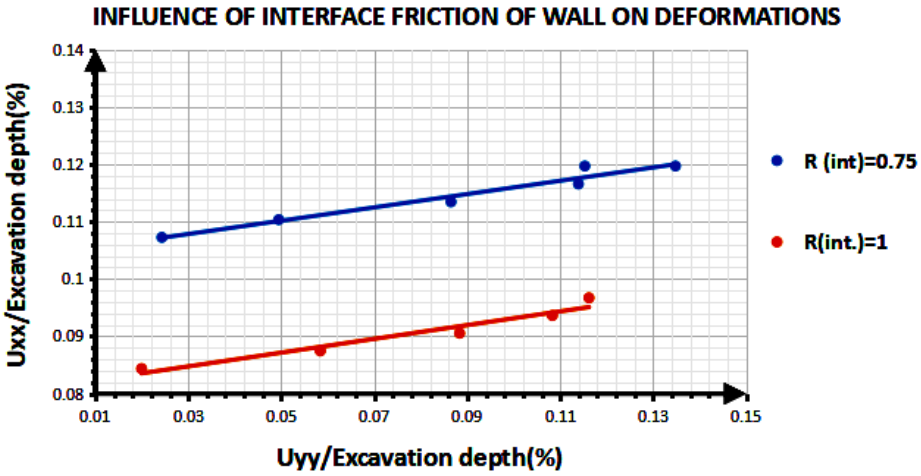

Fig. 8. Influence of interface friction of wall on deformations

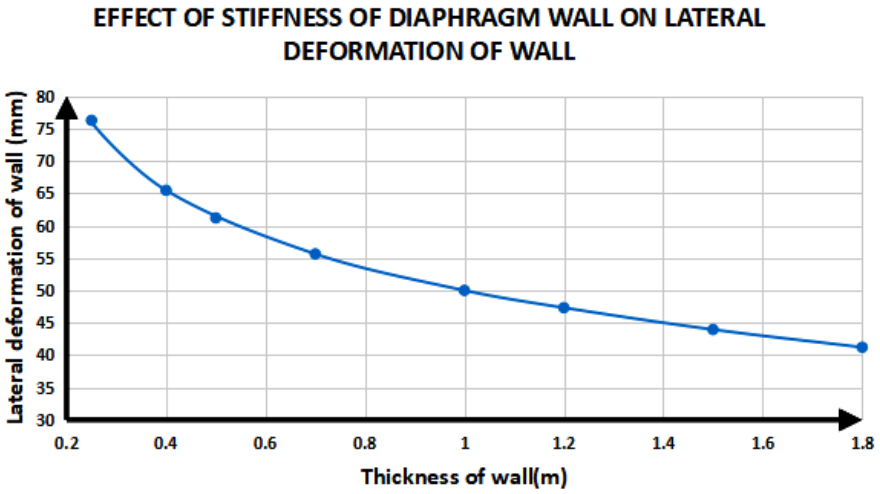

Fig.9. Effect of the stiffness of diaphragm wall on lateral deformation of the wall

6 Conclusions

1. Numerical modelling start with defining boundary conditions to model. In this study, the convergence method is defined to select boundary conditions in terms of

the width of excavation (B), Depth of excavation (De), Surface settlement, and lateral wall displacement. Finally, 8xB model size from both faces of the wall is selected as the effect of the boundary on the surface and lateral deformation of the wall start to cease.

2. The lateral deformation of support and surface settlement can be easily simulated with the use of the Plaxis at each excavation stage. The maximum lateral deformation observed in the Diaphragm wall is 50 mm and the maximum settlement observed is 26.53 mm.
3. It is observed that the influence of penetration depth in reducing the lateral deformation of the wall is inappreciable as only 4 mm reduction is observed when penetration depth reduced to 5.4 m from 16.4 m.
4. The influence of thickness in reducing the lateral deformation of the wall is inappreciable when the thickness of the wall is large. A 15 mm reduction is observed only when thickness increase to 1.8 m from 0.6 m, and 30 mm when it increases to 0.6 m from 0.2 m.
5. It is observed that when interface friction between the wall and interface soil is more, lesser deformations occurred. It means if the wall face towards soil is made rough, fewer deformations of the wall is there.
6. The optimum thickness of the wall, penetration depth can be predicted from the simulation results easily.

References

1. Bin-Chen Benson Hsiung: A case study on the behaviour of a deep excavation in sand, Computers and Geotechnics, 665–75 (2009).
2. Duncan JM, Chang C.: Nonlinear analysis of stress and strain in soils, Proc Pap: J Soil Mech Found Div ASCE, 1629–1653 (1970).
3. Kulhawy F, Mayne P.: Manual on estimating soil properties for foundation design, Palo Alto: Electric Power Research Inst., (1990).
4. Brinkgreve, R., Broere, W., & Waterman, D.: PLAXIS 2-D Professional Version - User's Manual, (2012).
5. Nikolinakou MA, Whittle AJ, Sadivis S, Schran U.: Prediction and interpretation of the performance of a deep excavation in Berlin sand, J Geotech Eng ASCE, (2011).
6. Calvello M, Finno RJ.: Selecting parameters to optimize in model calibration by inverse analysis, Computers, and Geotechnics, 410–24 (2004).
7. Schanz T, Vermeer PA, Bonnier PG.: The hardening soil model-formulation and verification, Computational Geotechnics, (1999).
8. Bowles JE.: Foundation analysis and design. 5th edn. McGraw-Hill, (1995).
9. Bolton MD.: The strength and dilatancy of sands, Geotechnique, 65–78 (1986).
10. Ou C-Y. Deep excavation: Theory and practice, Taylor & Francis, (2006).
11. Braja M. Das: Principles of Geotechnical Engineering. 1th edn. Cenage learning, (1994).